AEM
Journals.ASM.org

Differential Growth of and Nanoscale TiO_2 Accumulation in *Tetrahymena thermophila* by Direct Feeding versus Trophic Transfer from *Pseudomonas aeruginosa*

Randall E. Mielke,[a,b] John H. Priester,[a] Rebecca A. Werlin,[c] Jeff Gelb,[d] Allison M. Horst,[a] Eduardo Orias,[c] Patricia A. Holden[a]

Bren School of Environmental Science and Management, Earth Research Institute, and UC Center for the Environmental Implications of Nanotechnology (UC CEIN), University of California, Santa Barbara, California, USA[a]; Jet Propulsion Laboratory, California Institute of Technology—NASA, Planetary Science, Pasadena, California, USA[b]; Department of Molecular, Cellular and Developmental Biology, University of California, Santa Barbara, California, USA[c]; Xradia Corporation, Pleasanton, California, USA[d]

Nanoscale titanium dioxide (TiO_2) is increasingly used in consumer goods and is entering waste streams, thereby exposing and potentially affecting environmental microbes. Protozoans could either take up TiO_2 directly from water and sediments or acquire TiO_2 during bactivory (ingestion of bacteria) of TiO_2-encrusted bacteria. Here, the route of exposure of the ciliated protozoan *Tetrahymena thermophila* to TiO_2 was varied and the growth of, and uptake and accumulation of TiO_2 by, *T. thermophila* were measured. While TiO_2 did not affect *T. thermophila* swimming or cellular morphology, direct TiO_2 exposure in rich growth medium resulted in a lower population yield. When TiO_2 exposure was by bactivory of *Pseudomonas aeruginosa*, the *T. thermophila* population yield and growth rate were lower than those that occurred during the bactivory of non-TiO_2-encrusted bacteria. Regardless of the feeding mode, *T. thermophila* cells internalized TiO_2 into their food vacuoles. Biomagnification of TiO_2 was not observed; this was attributed to the observation that TiO_2 appeared to be unable to cross the food vacuole membrane and enter the cytoplasm. Nevertheless, our findings imply that TiO_2 could be transferred into higher trophic levels within food webs and that the food web could be affected by the decreased growth rate and yield of organisms near the base of the web.

With the increased production and use of manufactured nanomaterials, there are concerns regarding their environmental buildup and possible ecological impacts (1, 2). One highly produced nanomaterial is nanoscale titanium dioxide (TiO_2), which is found in a wide range of impermanent consumer products such as household paints (3, 4), cosmetics (5), medicinal ointments (6), and food products (7). On the basis of the projected increase in its production (8), manufactured TiO_2 will increasingly enter the environment, where it could impact ecosystem health (9), including food web interactions between protozoan predators and bacterial prey that are important in nutrient cycling (1).

Many manufactured nanomaterials (10), including TiO_2 (11) and either cadmium telluride (CdTe) (12) or cadmium selenide (CdSe) (13) quantum dots (QDs), have been shown to impact bacterial cell membranes and interfere with bacterial population growth (12, 13). In experiments with planktonic *Pseudomonas aeruginosa* growing in the presence of CdSe QDs, cell membranes were disrupted by reactive oxygen species, resulting in QDs entering cells (13–15). In a trophic-transfer experiment, we showed that intracellular CdSe QDs in *P. aeruginosa* prey were transferred into the ciliated protozoan predator *Tetrahymena thermophila* and biomagnified in the process (15). In another investigation, carbon nanotubes were directly ingested by these protozoans, which interfered with bactivory (ingestion of bacteria) (16), but trophic transfer was not studied. Thus, at least two scenarios of protozoan exposure to manufactured nanomaterials have been reported: protozoan predation upon bacteria with already internalized nanomaterials and direct ingestion of nanomaterials from the aqueous environment.

A third, potentially common, scenario for nanomaterial exposure to protozoans is via ingestion of nanomaterial-coated bacteria. While there are various potential nanomaterial impacts on bacteria according to nanomaterial properties, as well as exposure conditions (10), many nanomaterials such as TiO_2 are observed to adsorb to cell membranes, e.g., of *Escherichia coli* (11) and *P. aeruginosa* (17). In fact, since nanomaterials are often larger than typical bacterial cell wall openings (18), external envelope adsorption may be the prevalent mode of manufactured nanomaterial association with bacteria. Given this likelihood, questions arise concerning protozoan predation of such bacteria, i.e., if it occurs and whether bacterially sorbed nanomaterials, including TiO_2, can be transferred into protozoans during bactivory of nanomaterial-encrusted bacteria. Information about the trophic transfer of bacterially adsorbed TiO_2, with possible TiO_2 biomagnification in protozoa, will provide a better understanding of the potential impacts of manufactured TiO_2 on base food web interactions.

In this study, we investigated (i) whether TiO_2 that is adsorbed to *P. aeruginosa* is transferred to *T. thermophila* during protozoan bactivory and (ii) the possible effects on protozoan growth. The condition of *T. thermophila* grown with TiO_2-encrusted *P. aeruginosa* is compared to that of direct uptake of TiO_2, i.e., by *T. thermophila* grown in bacterium-free, nutrient-rich medium that is amended with TiO_2.

Received 22 May 2013 **Accepted** 3 July 2013
Published ahead of print 12 July 2013
Address correspondence to Patricia A. Holden, holden@bren.ucsb.edu.
Supplemental material for this article may be found at http://dx.doi.org/10.1128/AEM.01680-13.

doi:10.1128/AEM.01680-13

MATERIALS AND METHODS

Strains, media, and nanomaterials. The bacterial strain used in this study was *P. aeruginosa* PG201, a Gram-negative organism studied previously (13, 15, 17) and maintained at −80°C. As described before (15), the protozoan strain was *T. thermophila* SB210E. The medium used for *P. aeruginosa* cultivation was Luria Bertani (LB) broth or agar. The medium used for *T. thermophila* cultivation was either super-nutrient-rich medium (1% SSP [1% proteose peptone, 0.1% yeast extract, 0.2% dextrose, 75 μM Fe EDTA]) for growth experiments involving direct TiO_2 exposure or starvation medium (Dryl's medium [2 mM sodium citrate, 2 mM $NaH_2PO_4 \cdot H_2O$, 1 mM Na_2HPO_4, 1.5 mM $CaCl_2$, pH 7.4]) for trophic-transfer experiments.

The nanomaterial was dry powder industrial P25 Aeroxide TiO_2 (Evonik, Parsippany, NJ) (75% anatase and 25% rutile) (19), which was stored in the dark at room temperature prior to use. As described by Horst et al. (17), the industrial TiO_2 used in these experiments is highly heterogeneous, with equivalent particle diameters ranging from 6.4 to 73.8 nm, where 75% of the particles are between 15 and 60 nm (average diameter, 37.5 nm). The electrophoretic mobility (zeta potential) of this TiO_2 varies with aqueous chemistry (20) and in LB medium is −17.9 mV (17). All other chemicals were reagent grade or better (Sigma Chemical or Fisher Scientific). Nanopure water (pH 6.9, 18.2 MΩ-cm) was used to prepare media and nanomaterial suspensions.

Preparation of *P. aeruginosa* and *T. thermophila* inocula. The bacterial inoculum was initially streaked from frozen stock (−80°C, preserved in 70% LB plus 30% [vol/vol] glycerol) onto LB agar and cultivated in the dark (12 h, 30°C). Following incubation, several discrete colonies were dispersed into 4 ml of LB broth to serve as the liquid inoculum.

T. thermophila cells maintained axenically by passaging every 3 weeks in nutrient medium at room temperature were inoculated into standard (10 cm by 15 mm) sterile plastic petri dishes containing 10 ml SSP and grown in a humidity chamber without shaking (17 h, 30°C), similarly to before (15). After reaching mid to late exponential phase, the culture was centrifuged (1,470 × *g*, 40 s). The cell pellet was washed once with Dryl's medium, and cells were resuspended to a concentration of ca. 650,000 ml^{-1} in 10 ml of Dryl's medium in petri dishes and then starved (17 h, 30°C) in humidity chambers. The starved *T. thermophila* cells were centrifuged, washed in Dryl's medium, and resuspended in either SSP or Dryl's medium for growth experiments, including trophic-transfer studies (Dryl's medium only).

***P. aeruginosa* cultivation in liquid medium.** *P. aeruginosa* was cultured in LB broth to determine the effects of TiO_2 exposure on growth and the amount of TiO_2 adsorbed to the bacteria; identical *P. aeruginosa* cultivation conditions were used to generate prey for trophic-transfer experiments. Cultivation was performed similarly to before (17), i.e., in the dark in 96-well plates (flat-bottom polystyrene with clear bottom and sides; Corning Incorporated) with 200 μl of LB broth (with or without 0.1 mg TiO_2 ml^{-1}) per well and inoculation with exponential-phase *P. aeruginosa*. For the TiO_2 treatments, dry TiO_2 powder was preweighed, added to sterile LB broth, vortexed (10 min), dispensed into wells, and inoculated with *P. aeruginosa*. As before, TiO_2 handled in this way initially formed large agglomerates that dispersed during *P. aeruginosa* population growth because of the adsorption of TiO_2 onto *P. aeruginosa* surfaces (17). Each treatment (including uninoculated controls) was prepared in triplicate. The multiwell plates were incubated (30°C, 200 rpm) in a Synergy HT Multi-Mode microplate reader (Biotek Instruments, Winooski, VT) equipped with a xenon lamp set to measure optical density at 600 nm (OD_{600}) regularly over time.

P. aeruginosa cultures for use in *T. thermophila* feeding (trophic-transfer) experiments were prepared in glass flasks containing 400 ml of LB broth with or without 0.1 mg TiO_2 ml^{-1} and 25 μl of *P. aeruginosa* inoculum. The flasks were incubated in the dark at 30°C while shaking at 200 rpm until the OD_{600} reached 0.4 (ca. 10 h). The flask contents were dispensed (40-ml aliquots) into 10 50-ml tubes for centrifugation (12,000 × *g*, 10 min), and the supernatants were discarded. Each pellet was washed once with Dryl's medium to remove LB medium constituents and resuspended in 20 ml of sterile Dryl's medium. The washed cells for each treatment were combined, and triplicate (60-ml) aliquots from each flask were transferred into separate, sterile glass flasks from which 1 ml was removed for fixation and cell counting. The experiment was repeated identically to provide *P. aeruginosa* cells for imaging by environmental scanning electron microscopy (ESEM). The remaining cell suspensions, which, according to the above steps, consisted of a washed 2× concentration of the harvested culture, were used for *T. thermophila* feeding experiments. It was determined, by assessing the initial mass of TiO_2 administered to the *P. aeruginosa* culture versus the TiO_2 observed to be sorbed onto these bacteria (by ESEM; see the supplemental material), that all of the TiO_2 administered was sorbed to the bacteria at the start of the trophic-transfer experiment. Thus, there was no need to separate unbound TiO_2 from bacterially sorbed TiO_2 during culture washing.

***T. thermophila* growth without *P. aeruginosa* prey.** *T. thermophila* cells were cultivated in either SSP or Dryl's medium in the absence of *P. aeruginosa* prey to determine the effects of direct TiO_2 exposure on *T. thermophila* growth rates and yields. In the control cultures (without TiO_2), starved *T. thermophila* cells were suspended in 12 ml of either Dryl's or SSP medium in petri dishes. Where used, TiO_2 was first sonicated (10 W, 20 min, Branson 8210; Branson, Danbury, CT) and diluted to a final concentration of 0.10 mg ml^{-1} in 12 ml of either Dryl's or SSP medium, and then *T. thermophila* inocula were dispensed into the TiO_2 suspensions. In the control and TiO_2 treatments, the starting culture represented a 100× dilution of starved inocula to 6,500 cells ml^{-1}. Each inoculated culture (i.e., each medium with or without TiO_2) was established in triplicate. Abiotic controls consisted of uninoculated medium with or without TiO_2. *T. thermophila* cells were cultured in the dark at 30°C in a humidity chamber without agitation. The cultures were sampled over time for cell counting and observation of live-cell characteristics under a dissecting microscope. Cultivation was repeated within 1 day as described above but with enough replicates to allow for sacrificing of entire cultures at 2, 8, 16, and 22 h for use in Nomarski and electron microscopy.

***T. thermophila* growth with *P. aeruginosa* prey.** *T. thermophila* cells were cultured in Dryl's medium with *P. aeruginosa* to determine growth rates and yields when bacterial prey, with or without preadsorbed TiO_2, was the only food source. In the control *T. thermophila* growth experiment, control *P. aeruginosa* cells (cultured without TiO_2 for 10 h) were suspended in Dryl's medium as described above. Starved *T. thermophila* cells were added to achieve a final density of ca. 6,500 ml^{-1} as described before (15). The trophic-transfer and control growth experiments were conducted identically, except that *P. aeruginosa* cells used in trophic-transfer studies had presorbed TiO_2. Six individual replicate experiments were prepared—three each for the control and trophic-transfer experiments. All other cultivation conditions and approaches, including additional experimental replication for microscopy, were identical to the procedures used for *T. thermophila* cultured in SSP medium (without *P. aeruginosa*).

Cell counting by light microcopy. *P. aeruginosa* cells for counting were fixed with glutaraldehyde (2.5%, vol/vol) and stored at 4°C briefly (less than 24 h). Fixed cells were then stained with SYBR gold (Life Technologies, Carlsbad, CA) and counted by epifluorescence microscopy (Nikon E800, ×1,000 total magnification) as described before (13).

T. thermophila population growth was assessed for all of the cultures (with or without, *P. aeruginosa* prey or TiO_2) by counting the cells in a 100-μl sample (fixed with 5 μl formaldehyde) periodically (2, 4, 8, 16, and 22 h) with a hemocytometer. Duplicate counts were averaged for each time point. For differential interference contrast (Nomarski) imaging of *T. thermophila* morphology, 1.5 ml of each *T. thermophila* culture was fixed with glutaraldehyde to a final concentration of ~2.5% (vol/vol). An aliquot (50 μl) was imaged at 200× magnification by Nomarski bright-field microscopy. *T. thermophila* cells were also observed periodically dur-

ing population growth for overall morphology and swimming behavior (without fixing) with a dissecting microscope.

Electron microscopy and X-ray microanalysis. Electron microscopy was used to image TiO_2 on *P. aeruginosa* and within *T. thermophila* cells. TiO_2 uptake into *T. thermophila* cells was quantified by digitally analyzing electron micrographs. This, in turn, allowed calculations of TiO_2 bioconcentration and biomagnification.

Imaging by ESEM was used to confirm that TiO_2 was adsorbing to *P. aeruginosa* cell membranes as described before (17). The washed bacteria were imaged directly on a carbon-coated aluminum stub with an FEI Co. XL30 field emission gun (FEG) environmental scanning electron microscope (Philips Electron Optics, Eindhoven, The Netherlands) at a 20-kV accelerating voltage with a gaseous secondary electron detector in the wet mode (4 torr) and a 10.3-mm working distance. This method had been independently confirmed previously (by cryoscanning electron microscopy and by dynamic light scattering of *P. aeruginosa* cells) to reliably enable visualization of *P. aeruginosa* cells retaining a tightly adsorbed TiO_2 coating on cellular outer membranes (17).

Imaging by scanning transmission electron microscopy (STEM) was used for high-magnification observations of *T. thermophila*, including internalized TiO_2. To prepare *T. thermophila* cells for STEM imaging and analysis, 10 ml of each *T. thermophila* culture was fixed with glutaraldehyde to a final concentration of ~2.5% (vol/vol) and then refrigerated (4°C) until embedding. The 10-ml fixed samples were prepared for embedding by centrifugation (10,000 × *g*, 10 min), followed by three sequential washings with 500 μl of nanopure water. The cell pellet was combined with 50 μl of 2% Noble agar and extruded as an agar worm; this was followed by optional staining (1 h) with 2% OsO_4 (15). Both stained and unstained specimens were prepared. The stained and unstained specimens were then sequentially dehydrated with 25%, 50%, 75%, and 2× 100% ethanol at intervals of 15 min. The dehydrated samples were infused with 1:1 ethanol-acetone and 100% acetone at 15-min intervals, followed by a final 8-h infusion of 1:1 acetone-resin at 4°C. The specimen agar worms were transferred into molds with 100% Eponate 12 resin and dried (60°C, 24 h) (15). The samples in resin blocks were sectioned with an ultramicrotome with a 45° Diatome diamond knife. The ultrathin sections (60 nm) were deposited on Formvar-coated 200-mesh copper grids (15). Imaging was performed with an FEI XL30 FEG environmental scanning electron microscope (Philips Electron Optics, Eindhoven, The Netherlands) at a 30-kV accelerating voltage with a STEM detector in high-vacuum mode at an ~6.7-mm working distance. All images were dark field with minimal digital postprocessing.

ESEM was also used to evaluate TiO_2 distribution within *T. thermophila* cultured in trophic-transfer experiments. Selective embedded samples were thick sectioned (5 μm) and deposited onto sticky carbon dots (Ted Pella, Redding, CA) adhering to 100% silicon slides (1 by 1 cm; Electron Microscopy Sciences, Hatfield, PA) (21). The thick sections were imaged by ESEM (as described above) in the wet mode (4 torr) and at a 10.3-mm working distance at a 20-kV accelerating voltage with a backscatter secondary electron detector.

To confirm the presence and location of elemental titanium (Ti) in thick sections, energy-dispersive X-ray spectroscopy (EDS) of selected areas of either 1-μm^2 (ESEM) or 100-nm^2 (STEM, data not included) areas was performed with an X-ray spectrometer (15 s at 25.6 μS) with a sapphire Super Ultra-Thin Window (EDAX, Inc., Mahwah, NJ) on an FEI Nano600 FEG microscope (15). Genesis analytical software (EDAX, Inc.) was used in conventional atomic number, absorption, and fluorescence (ZAF) correction mode to analyze the spectra (15), i.e., to obtain atomic mass percentages for titanium along with additional elements (C, O, Si, P, S, Cl, K, Ca) (22).

X-ray microscopy. X-ray microscopy was used to visualize the TiO_2 metal (Ti) distribution in *T. thermophila* cells. A resin-embedded thick section (50 μm) of *T. thermophila* cells (harvested after 22 h of growth on TiO_2-encrusted *P. aeruginosa*) was mounted to a thin wire for imaging with an Xradia UltraXRM-L200 3-D (Xradia, Inc., Pleasanton, CA) microscope with a quasimonochromatic operating photon energy of 8 keV, configured with a 65-μm isotropic field of view at a 150-nm spatial resolution (23). The Zernike phase-contrast imaging mode was used to enhance the visualization of TiO_2 within *T. thermophila* food vacuoles (24). A tomography series was created from transmission X-ray images collected at 0.2° steps across a 180° rotation range with a 4-min integration time per image. The Xradia XMReconstructor software package was used to reconstruct the tomography series into a stack of tomograms corresponding to virtual slices inside the specimen by the filtered back projection reconstruction technique. The Xradia XM3DViewer software assembled these tomograms into various renderings to visualize the area imaged in both planar and three-dimensional (3D) volumetric formats.

Calculation of TiO_2 mass adsorbed to *P. aeruginosa*. The mass of TiO_2 adsorbed to *P. aeruginosa* cells was calculated by assuming, and then confirming via ESEM images, that all of the TiO_2 administered became adsorbed to *P. aeruginosa* bacterial cells during growth. The mass of TiO_2 per *P. aeruginosa* cell was divided by the calculated cell volume and the dry cell mass to estimate the volume- and mass-based concentrations of TiO_2 delivered with prey cells during *T. thermophila* predation of TiO_2-encrusted *P. aeruginosa* (see the supplemental material). The volumetric concentration of TiO_2 on *P. aeruginosa* cells was used to calculate the biomagnification factor (BMF) associated with TiO_2 trophic transfer from *P. aeruginosa* into *T. thermophila*. Note that since the TiO_2 nanoparticles administered here greatly exceed the size of typical bacterial cell envelope openings (18) and since TiO_2 thus was only extracellularly adsorbed onto *P. aeruginosa* cells, there was no basis for the calculation of a bioconcentration factor (BCF) for *P. aeruginosa* uptake of TiO_2.

Quantitative analysis of *T. thermophila* food vacuoles. For *T. thermophila* cells grown either directly with TiO_2 (SSP medium) or with TiO_2-encrusted *P. aeruginosa* (in Dryl's medium), *T. thermophila* food vacuole geometries and the amounts of TiO_2 that accumulated in food vacuoles were measured by quantitative analysis of STEM images. The image measurements, made with the Measurement Tool in Adobe Photoshop, were of the food vacuole diameters and areas and also the areas in the food vacuoles that were TiO_2 dense as evidenced by image brightness. Between three and eight *T. thermophila* cells and between 9 and 23 food vacuoles were analyzed at each time point. The number of visible food vacuoles per cell varied, as this depended on the plane of the section created when specimens embedded in random orientations were microtomed for STEM imaging. At each time point, the diameters of up to seven randomly selected food vacuoles were measured for each image. Because the food vacuoles appeared to be circular, the area of each was calculated by assuming circular geometry. The areas of the same food vacuoles were then measured directly in Adobe Photoshop with the Area Measurement Tool. The directly measured areas were compared to the calculated areas to determine if the assumption of circular geometry, and thus spherical geometry for volume calculations, was legitimate.

With the Area Select and Measurement Tools in Photoshop, the area of TiO_2 filling within each of the same food vacuoles was measured as described above after adjusting the image brightness to retain only the bright, electron-dense (TiO_2-enriched) regions of each food vacuole. The total measured bright area was typically irregularly shaped and often consisted of multiple irregular subareas. Still, the total measured area was converted to a circular geometry so that a volume could be calculated by assuming spherical geometry. The assumption of spherical geometry is justified by the observation that, in sections of many cells at random angles, food vacuoles always showed a nearly circular cross section. The equivalent diameter (D_{ti}; see Fig. S1 in the supplemental material) of a circle whose area was equivalent to the measured area, A_{Ti} (see Fig. S1), was calculated by using the equation for a circle. Relating the equations for a circle and a sphere to one another, the volume of TiO_2 filling was calculated as $V = 4/3\ r\ A_{Ti}$, where the radius r equals $D_{Ti}/2$. The volume calculation thus required the assumption that the TiO_2 in food vacuoles propagated depthwise into and out of the plane of the imaged embedded specimen section. Since this assumption would likely generate an overes-

timate of TiO_2 in the food vacuoles, calculations of bioconcentration and biomagnification were also likely overestimates. The percentage by volume of the food vacuole that was filled with TiO_2 was then calculated (see Fig. S1 and Table S1 in the supplemental material). The mass of TiO_2 per food vacuole was also calculated by multiplying the TiO_2 volume of each food vacuole by the TiO_2 density of 3.97 g cm^{-3} (17). The mass of TiO_2 per *T. thermophila* cell was estimated by assuming that there were seven TiO_2-containing food vacuoles (at all of the sampling points) per cell, on the basis of a 3D X-ray volume rendering (see Movie S1 in the supplemental material). The *T. thermophila* cellular concentration of TiO_2 was then estimated by assuming a constant cell volume of 7,042 μm^3, as measured before (15). These measured and calculated variables are summarized in Table S1 and shown as a graphical scheme in Fig. S1 in the supplemental material.

Bioconcentration and biomagnification calculations. BCFs of TiO_2 in *T. thermophila* cells grown in SSP medium were calculated at 2, 8, 16, and 22 h by dividing the cellular TiO_2 concentration by the TiO_2 concentration in the medium. There were two key assumptions in making the *T. thermophila* BCF calculations. The first was that TiO_2 in *T. thermophila* cells was only within the food vacuoles. This was confirmed by inspection of STEM images and EDS data acquired in *T. thermophila* cytoplasm external to the food vacuoles. The second was that the medium TiO_2 concentration was decreased from the initial concentration by the amount of TiO_2 accumulated in the *T. thermophila* population at each time point.

The BMFs at 2, 8, 16, and 22 h for *T. thermophila* cells feeding on TiO_2-encrusted *P. aeruginosa* cells were calculated by dividing the *T. thermophila* cellular TiO_2 mass concentration by the P. *aeruginosa* cellular TiO_2 mass concentration, where both cellular mass concentrations were on a dry cell mass basis (25, 26).

Quantitative assessment of TiO_2 within *T. thermophila* populations. The amounts of TiO_2 within whole *T. thermophila* populations at each time point were calculated by combining the *T. thermophila* cell concentrations with the TiO_2 masses in food vacuoles (and therefore *T. thermophila* cells) that were measured by quantitative image analysis. Mass values were calculated at each time point by multiplying the TiO_2 mass per *T. thermophila* cell by the population size (the number of *T. thermophila* cells per milliliter of culture) and by 12 ml (culture volume in *T. thermophila* growth experiments). Percentages were calculated at each time point by dividing the masses by the total TiO_2 administered in the 12 ml of *T. thermophila* culture medium (1.2×10^9 pg for SSP, 2.16×10^9 pg for Dryl's medium plus TiO_2-encrusted *P. aeruginosa*) and then multiplying each fraction by 100.

Additional data and statistical analyses. Exponential growth rate constants for *P. aeruginosa* and *T. thermophila* cells were calculated from the slopes of the best-fit (by linear regression) lines through log-transformed OD_{600} (*P. aeruginosa*) or cell count (*T. thermophila*) time course data for each replicate in each growth experiment with Microsoft Excel 2010 software. Statistical analyses of the replicate results were performed with SPSS 12.0.1 (SPSS Inc., Chicago, IL) or Microsoft Excel 2010 software. Means were compared by the Student *t* test or by one-way analysis of variance.

RESULTS

Growth and morphology of *P. aeruginosa*. Planktonic *P. aeruginosa* grew exponentially with or without TiO_2 (see Fig. S2 in the supplemental material). The specific growth rates averaged 0.97 ± 0.11 h^{-1} and 0.97 ± 0.06 h^{-1} in the control and TiO_2 treatments, respectively; these values did not significantly differ (*t* test, $P = 0.50$), which indicated that TiO_2 was not growth inhibitory and did not interfere with OD_{600} measurements. ESEM micrographs of *P. aeruginosa* cells cultivated with TiO_2 showed extracellular bright accumulations on the cells, confirming the adsorption of electron-dense Ti onto their cell membranes (see Fig. S3 in the supplemental material).

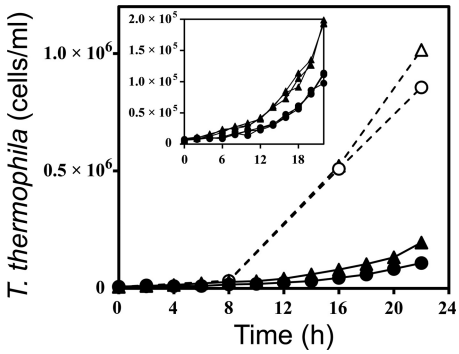

FIG 1 Growth curves of *T. thermophila* cultured in rich (SSP) medium without *P. aeruginosa* prey (open symbols, dashed lines) or in Dryl's medium with bacterial prey (closed symbols, solid lines). Triangles (△, ▲) and circles (○, ●) represent control treatment (without TiO_2) and treatment with TiO_2, respectively. Each point is the average of three independent replicates. Standard-error bars are smaller than the symbols and thus not visible. The inset graph shows the individual replicate growth curves for the six Dryl's medium (with prey) cultures. The symbols in the inset represent the same treatments as in the main graph.

***T. thermophila* growth and motility.** *T. thermophila* cells grew rapidly in rich (SSP) medium with or without TiO_2 (Fig. 1). Exponential growth occurred over 16 h; the associated *T. thermophila* specific growth rate averaged 0.26 ± 0.003 h^{-1} and was the same with or without TiO_2 ($P = 0.17$). The maximum cell counts (22 h; Fig. 1) were approximately 19% lower when TiO_2 was present than in the control, and the difference was significant ($P = 0.00$). As expected, there was no growth in Dryl's medium in the absence of *P. aeruginosa* as prey, with or without TiO_2 (data not shown).

By staining and direct counting, the initial concentration of *P. aeruginosa* cells in *T. thermophila* trophic-transfer experiments was 3.6×10^9 ml^{-1}. The growth of the *T. thermophila* predator population was exponential over 22 h (Fig. 1; see Fig. S4 in the supplemental material), and the associated specific growth rate of the protozoans consuming control prey (i.e., no adsorbed TiO_2) averaged 0.14 ± 0.00 h^{-1} ($n = 3$). This specific growth rate was 7% higher than the average specific growth rate of the protozoans eating prey that had preadsorbed TiO_2 (0.13 ± 0.00 h^{-1}, $n = 3$), and the difference between the two treatments was significant ($P = 0.03$). Growth of *T. thermophila* with TiO_2-encrusted *P. aeruginosa* resulted in a 45% reduction in the 22-h protozoan cell count compared to that of *T. thermophila* with control *P. aeruginosa* ($P = 0.00$; Fig. 1). As expected, growth of *T. thermophila* in Dryl's medium when *P. aeruginosa* prey was the exclusive food source was slower than in SSP, with or without TiO_2 (Fig. 1). The final (22-h) protozoan cell count in Dryl's medium with *P. aeruginosa* was lower by approximately 81% without TiO_2 ($P = 0.00$) and by approximately 89% with TiO_2 ($P = 0.00$) than that in rich (SSP) medium (no bacteria). When considering the initial counts of *P. aeruginosa* prey (4.3×10^{10} cells, i.e., 3.6×10^9 cells ml^{-1} in 12 ml; see the supplemental material) and assuming a yield of 2×10^{-5} *T. thermophila* cells per *P. aeruginosa* cell as described before (15), the maximum expected *T. thermophila* population size was 8.6×10^5 cells per culture or 7.2×10^4 cells ml^{-1}. This is a slightly lower *T. thermophila* cell concentration than that measured in this experiment at 22 h (Fig. 1), suggesting that the *T. thermophila* populations in this trophic-transfer experiment were likely in late exponential phase by 22 h.

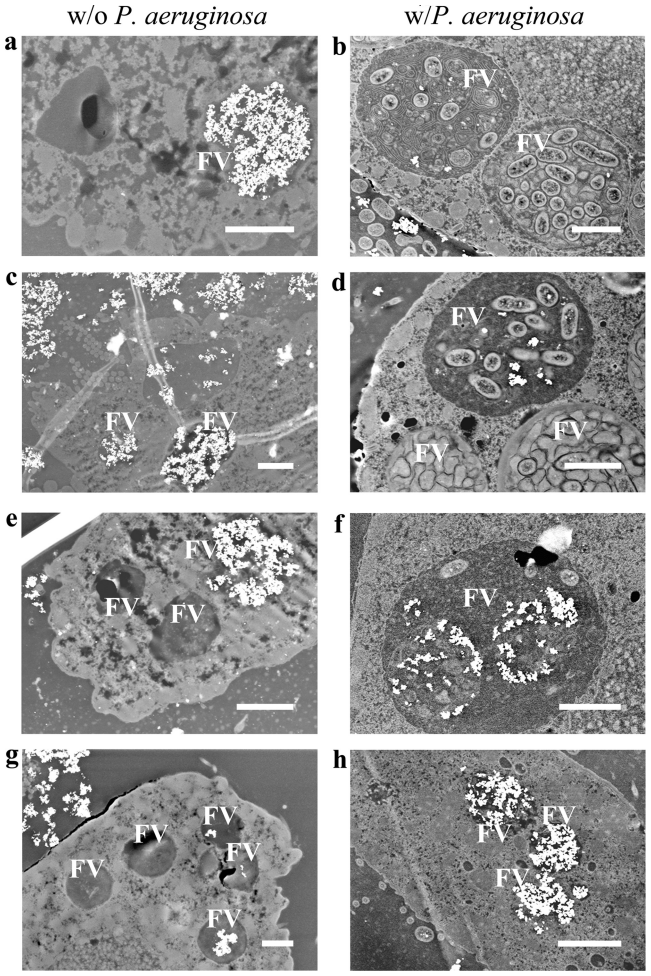

FIG 2 Dark-field STEM micrographs of unstained thin sections of *T. thermophila* cells grown in rich medium (SSP) in the presence of TiO_2 (0.1 mg ml^{-1}) without (w/o) bacteria (left column) or in Dryl's medium with (w) TiO_2-encrusted *P. aeruginosa* prey (right column). *T. thermophila* cells are shown after 2 h (a, b), 8 h (c, d), 16 h (e, f), and 22 h (g, h) of growth, where 16 and 22 h were during rapid growth (Fig. 1). Food vacuoles (FV) are indicated. The brighter spots are indicative of higher-molecular-weight elements, in this case, Ti associated with TiO_2. Scale bars, 2 μm.

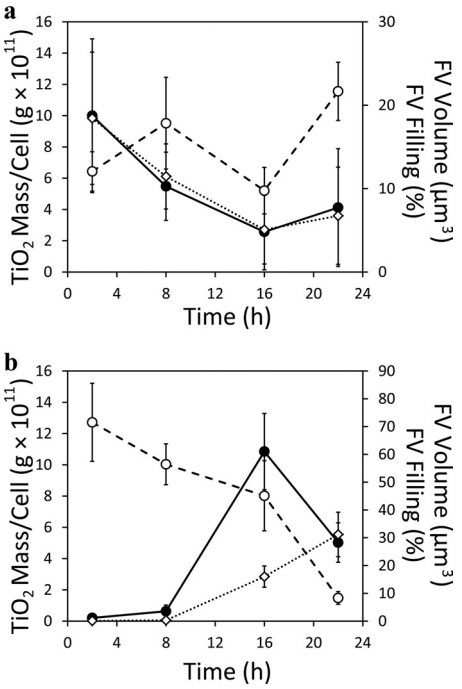

FIG 3 Time course during *T. thermophila* growth (Fig. 1) of mean food vacuole (FV) volume (○, dashed lines), measured average percent food vacuole volume filled with TiO_2 (◇, dotted lines), and TiO_2 mass per *T. thermophila* cell (●, solid lines). (a) *T. thermophila* grown in rich (SSP) medium with 0.1 mg ml^{-1} TiO_2 but without *P. aeruginosa* bacterial prey. (b) *T. thermophila* grown by feeding exclusively on TiO_2-encrusted *P. aeruginosa* cells. The patterns are consistent with those observed in electron micrographs (Fig. 2). The plotted values are tabulated in Tables S2 to S5 in the supplemental material.

Light and Nomarski microscopy of control *T. thermophila* cells grown in SSP showed normal, vigorously swimming cells. Observations of the protozoans grown in the trophic-transfer experiments with *P. aeruginosa* showed physically normal *T. thermophila* cells swimming comparatively slower than cells growing in SSP. The swimming characteristics, grazing behavior, and physical appearance of *T. thermophila* cells remained similar throughout the 22-h experiment in all of the treatments. Thus, no obvious signs of TiO_2-induced morbidity of *T. thermophila* cells were observed under light microscopy in any of the treatments.

***T. thermophila* uptake of TiO_2 in rich medium.** For *T. thermophila* grown in SSP medium with TiO_2, the bright white spots in the unstained specimen STEM images show the presence of TiO_2 in food vacuoles at all of the time points, although there are temporal variations in TiO_2 accumulation (Fig. 2). The 2- and 8-h samples showed abundant TiO_2 accumulations in food vacuoles (Fig. 2a and c), indicating that *T. thermophila* was engulfing TiO_2 along with organic nutrients from the SSP medium (see Fig. S5 in the supplemental material). The 16- and 22-h samples showed smaller amounts of TiO_2 in food vacuoles (Fig. 2e and g). These trends are supported by the data obtained via quantitative image analysis (Fig. 3a; see Table S2 in the supplemental material). The TiO_2 available for consumption in the medium surrounding *T. thermophila* cells was apparent at 22 h (upper left corner, Fig. 2g) and also at 16 h (not shown). Consistent with the images of food vacuoles over time (Fig. 2), the calculated food vacuole volumes increased between 2 and 8 h, decreased at 16 h, and then increased again at 22 h (Fig. 3a; see Table S2). The TiO_2 mass per *T. thermophila* cell was highest at 2 h and then decreased until 16 to 22 h (Fig. 3a; see Table S4). The percent filling of food vacuoles by TiO_2 declined in a similar pattern (Fig. 3a). Still, although the overall TiO_2 mass per *T. thermophila* cell declined over time (Fig. 3a; see Table S4), the total TiO_2 in the *T. thermophila* population increased over time while the population size grew (Fig. 4). The final TiO_2 mass within the entire population was 0.42 mg (Fig. 4, top), which was ca. 35% of the total initial TiO_2 mass administered (Fig. 4, bottom).

***T. thermophila* uptake of TiO_2 from *P. aeruginosa* prey.** STEM images, acquired at 2, 8, 16, and 22 h, of unstained samples of *T. thermophila* grown exclusively by feeding on TiO_2-encrusted *P. aeruginosa* in Dryl's medium showed increasing amounts of TiO_2 in food vacuoles over time (Fig. 2). Normal digestion of *P. aeruginosa* cells in *T. thermophila* was indicated by the few observable *P. aeruginosa* cells in food vacuoles. Greater TiO_2 amounts, with still fewer undigested *P. aeruginosa* cells in food vacuoles,

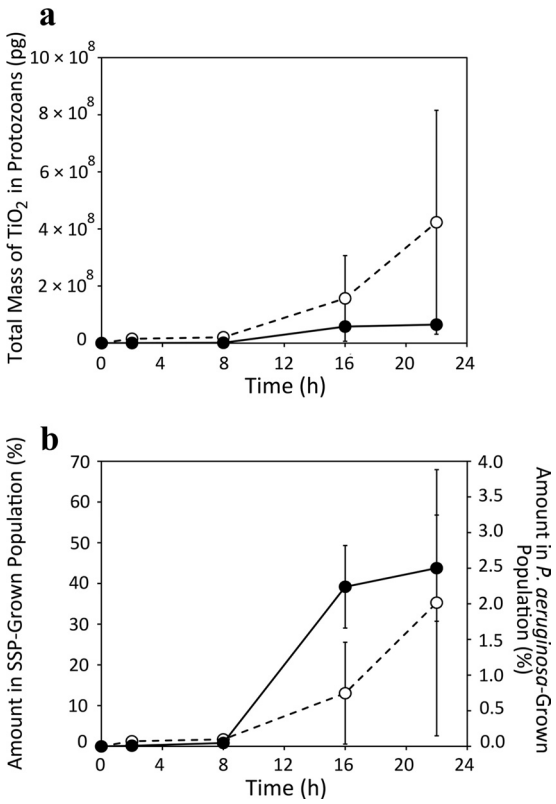

FIG 4 Total TiO_2 mass (a) and percentage of total administered TiO_2 (b) within whole *T. thermophila* populations at each time point during growth. Dashed line (○), SSP-grown population; solid line (●), population grown in Dryl's medium with *P. aeruginosa*. Points are average values ($n = 3$). Error bars are the result of propagating errors according to standard methods.

were observed at 16 h than at earlier time points (Fig. 2f). ESEM imaging showed TiO_2 bound to *P. aeruginosa* cell membranes within a *T. thermophila* food vacuole at 16 h (see Fig. S6 in the supplemental material); control (i.e., not TiO_2 exposed) treatments did not exhibit this brightness (not shown). The EDS spectrum (see Fig. S6) confirmed the presence of titanium. At 22 h, most food vacuoles appeared to be filled with TiO_2 and there were very few undigested *P. aeruginosa* cells (Fig. 2h). X-ray microscopy images of a thick section of a *T. thermophila* cell cultured to 22 h with TiO_2-encrusted *P. aeruginosa* cells as prey show, consistent with the STEM image (Fig. 2h), food vacuoles filled with TiO_2 mainly near the oral apparatus (see Fig. S7 and Movie S1 in the supplemental material). Nomarski images taken at 22 h also show numerous dark food vacuoles, illustrating that they contained TiO_2 (see Fig. S8).

The volume fraction of TiO_2 in food vacuoles varied with time when *T. thermophila* grown in SSP with TiO_2 was compared with *T. thermophila* grown with TiO_2-encrusted *P. aeruginosa* (Fig. 3). Initially (2 h), the food vacuoles of *T. thermophila* that were fed TiO_2-encrusted *P. aeruginosa* contained little TiO_2 (Fig. 3b; see Table S3). Over time, however, the amount increased (Fig. 3b; see Table S3). Essentially, the food vacuole-filling patterns were reversed for *T. thermophila* grown in TiO_2-amended SSP and *T. thermophila* grown with TiO_2-encrusted *P. aeruginosa* (Fig. 3; see Table S2 versus S3).

The average food vacuole volume decreased rather consistently between 2 and 22 h for *T. thermophila* cells feeding exclusively on TiO_2-encrusted *P. aeruginosa* (Fig. 3b; see Table S3), while the volume percent of food vacuoles filled with TiO_2 increased (Fig. 3b). The calculated mass of TiO_2 per *T. thermophila* cell increased between 2 and 16 h for *T. thermophila* feeding on TiO_2-encrusted *P. aeruginosa* but then dropped at 22 h to less than half of the 16-h value (Fig. 3b; see Table S5). Although *T. thermophila* population growth still appeared to be exponential between 16 and 22 h (Fig. 1; see Fig. S4), the total TiO_2 in this predatory *T. thermophila* population peaked at 16 h and was 0.06 mg at 22 h (Fig. 4, top). This final mass of TiO_2 in the *T. thermophila* population represented less than 3% of the starting TiO_2 mass associated with *P. aeruginosa*-encrusted cells (Fig. 4, bottom).

Quantitative assessment of TiO_2 bioconcentration and biomagnification. The mass of TiO_2 adsorbed per *P. aeruginosa* cell was determined to be 0.06 pg (see Section 1.2 of the supplemental material). On a dry cell mass basis and on a cell volume basis, this is equivalent to 0.33 pg of TiO_2/pg of TiO_2-encrusted dry *P. aeruginosa* cells and 0.00015 mg of TiO_2/ml of *P. aeruginosa* cells, respectively. All of the TiO_2 administered in the trophic-transfer growth medium was adsorbed to *P. aeruginosa* cells (see the supplemental material).

For *T. thermophila* grown in rich medium with TiO_2, the cellular mass concentration of TiO_2 (Fig. 3a; see Table S4) declined from 2 to 22 h. During the growth time course, the cellular TiO_2 made up 5% or less of the *T. thermophila* cell mass (see Table S4). The *T. thermophila* BCFs, calculated by dividing the *T. thermophila* cellular TiO_2 mass concentration by the initial SSP medium TiO_2 concentration, were 142, 78, 40, and 98 at 2, 8, 16, and 22 h, respectively (see Table S4). By these BCFs, TiO_2 was bioconcentrated in *T. thermophila* cells apparently only in the food vacuoles (Fig. 2) and not in the growth medium. However, its bioconcentration varied over time (see Table S4), as evidenced by the initially TiO_2-enriched and then TiO_2-depleted and enriched-again food vacuoles over time (Fig. 2 and 3a; see Table S2).

In *T. thermophila* grown by predation of TiO_2-encrusted *P. aeruginosa*, the *T. thermophila* cellular mass concentration of TiO_2 (Fig. 3b; see Table S5) increased from 2 and 8 h to 16 h and then decreased at 22 h. In the 2- to 22-h growth period, the TiO_2 mass per *T. thermophila* cell was up to 5% of the *T. thermophila* mass (see Table S5). When taking into account the cellular concentration of TiO_2 on TiO_2-encrusted *P. aeruginosa* prey (0.06 pg of TiO_2/pg of TiO_2-encrusted *P. aeruginosa* cells; see the supplemental material), the BMF was much less than 1, i.e., with a low of 0.003 at 2 h and a high of 0.16 at 16 h (see Table S5). Thus, TiO_2 was far more concentrated on *P. aeruginosa* cells than in *T. thermophila* cells. The low BMFs are partly explained by the volumetric dilution of initially bacterially associated TiO_2 into the much larger protozoan cells (i.e., 7,042 μm^3 for a *T. thermophila* cell versus 0.4 μm^3 for a bare *P. aeruginosa* cell; see Section 1.3 of the supplemental material) and also by the observation that TiO_2 stayed within food vacuoles and was not distributed into the *T. thermophila* cytoplasm (Fig. 2). The localization of ingested TiO_2 to food vacuoles within *T. thermophila* also limited biomagnification, as food vacuoles ultimately excrete their contents into the medium. Assuming that the yield of *T. thermophila* from predation upon control *P. aeruginosa* was ca. 2×10^{-5} protozoans per *P. aeruginosa* cell, as described before (15), the maximum potential mass of TiO_2 in the *T. thermophila* population would be (1.95×10^5 *T. thermophila* cells) × (2×10^5 *P. aeruginosa* cells/*T. thermophila*

cell) × (0.06 pg of TiO_2/*P. aeruginosa* cell) = 0.23×10^{10} pg or 2.33 mg of TiO_2. This maximum potential TiO_2 mass delivered into the *T. thermophila* population after 22 h of predation of TiO_2-encrusted *P. aeruginosa* is very close to the total TiO_2 initially associated with *P. aeruginosa* in the trophic-transfer experiment (2.6 mg; see Section 2 of the supplemental material). Clearly, since a much smaller mass of TiO_2 was in the *T. thermophila* population by 22 h (0.06 mg, Fig. 4), ingestion of TiO_2 via predation of TiO_2-encrusted *P. aeruginosa* had to have been accompanied by extensive TiO_2 excretion from *T. thermophila* food vacuoles. Thus, although food vacuoles were smaller and more TiO_2 filled over time (Fig. 3b), which may have contributed to a lower growth rate (Fig. 1), TiO_2 biomagnification did not occur in predatory *T. thermophila*, owing to localization of TiO_2 limited to *T. thermophila* food vacuoles, a cellular volumetric dilution effect, and ongoing excretion of TiO_2 back into the medium.

DISCUSSION

Given the prevalence and increasing use of nanoscale TiO_2 in consumer goods (8), it is potentially concerning that nanoscale TiO_2—a relatively insoluble manufactured nanomaterial—will accumulate in the environment, where microbial processes contributing to nutrient cycling could be impacted. Concentrations of nanoscale titanium were recently reported to be up to 6% in aquatic sediments near the outlet of a major wastewater treatment plant outfall (27). In the present study, a model protozoan, *T. thermophila*, was exposed to lower concentrations of TiO_2 via one of two routes, direct ingestion from surrounding aqueous medium or predation of TiO_2-encrusted bacterial prey, in this case, *P. aeruginosa* that had previously been shown to extracellularly adsorb TiO_2 (17). The results showed that the effects of TiO_2 on *T. thermophila* could vary with the exposure route.

Protozoans could be exposed to nanoscale TiO_2 in the environment via either medium or prey, and our results suggest TiO_2 uptake in either case. Protozoans accumulate nutrients by swimming through the water column and grazing along the solid-water interface (28), feeding on bacteria, inert materials, and other dead or decaying debris small enough to enter the oral apparatus (29, 30). Here, TiO_2 was ingested indiscriminately by *T. thermophila*. This was evidenced by the observation that the amount of nanomaterial taken up was quantitatively similar to the mass expected on the basis of the numbers of bacteria in the food vacuoles. For example, an 8-h food vacuole shows around 10 bacterial cells (Fig. 2d). This number of cells would have carried approximately 0.6 pg of TiO_2 (10 cells, each with 0.06 pg TiO_2; see Section 1 of the supplemental material) into the food vacuole, which is comparatively very close to the average mass of TiO_2 per food vacuole (0.9 pg; see Table S3). This indicates that there was no preferential feeding, e.g., of sparsely versus heavily coated *P. aeruginosa* cells. While there are prior examples of preferential feeding by protozoa, including an acidophilic protozoan that preferentially consumed *Acidithiobacillus ferrooxidans* over *Leptospirillum ferrooxidans* (31, 32) and marine protozoa that preferentially grazed on larger allochthonous bacteria even within a larger population of small autochthonous bacteria (33), other results are more similar to ours, i.e., showing predator-prey behavior with bacterially sorbed or free-floating particles and no preferential feeding with either inert beads (34) or CdSe ZnS-capped QD nanoparticles (35).

In a prior study conducted similarly, the trophic transfer of CdSe QDs resulted in significant toxicity to *T. thermophila* at the cellular and population levels, owing to the inherent chemical toxicity of the nanomaterials and the translocation of the QDs past food vacuoles and into the *T. thermophila* cytoplasm (15). In contrast, there were no obvious toxic cellular effects (as indicated by normal *T. thermophila* morphology and motility) of nanoscale TiO_2. Rather, effects were restricted to population growth. While the exact mechanism was not elucidated in this study, TiO_2 uptake into food vacuoles could displace nutrients and thereby create a nutrient-limiting condition that has an effect at the population scale, i.e., slightly slowing population growth for predatory *T. thermophila* exclusively fed TiO_2-encrusted *P. aeruginosa*. A consequence of this occurrence in nature could be a negative effect on the predator-prey equilibrium, which has inherent ecosystem level implications. This consideration would not have been predicted by the lack of observed toxicity to individual cells.

The potential for nanomaterial uptake into organisms and enhanced transfer of nanomaterials in food chains, i.e., bioaccumulation and biomagnification, is also of interest in the ecotoxicology of nanomaterials (15, 36). In a prior study, Cd associated with CdSe QDs was biomagnified during trophic transfer from *P. aeruginosa* to *T. thermophila* (15), suggesting that bacteria with their bioconcentrated nanomaterials could initiate biomagnification at the base of food webs. Nanomaterial uptake into bacteria has been demonstrated for gold (37), silver (38), cerium dioxide (CeO_2) (39), and CdSe QDs (13), as well as clays and other nanomaterials that tend to aggregate in nature (40, 41). However, here, while *T. thermophila* fed upon TiO_2-encrused *P. aeruginosa* and thereby ingested TiO_2, there was no quantitative biomagnification. In an analogous study of zebrafish that were ingesting TiO_2 either directly or by predation upon TiO_2-contaminated daphnids, the BCFs and BMFs were in the ranges of those reported here (42). In this study, since TiO_2 in *T. thermophila* cells was confined within food vacuoles, there was little opportunity for nanoscale TiO_2 to be magnified in these protozoans. With other nontoxic nanoscale metals, biomagnification does not occur since the predator-prey interactions facilitate metal recycling. For example, many iron-encrusted microbial communities are continually being grazed on by protozoa (43, 44) and the iron is ultimately utilized in protozoan and bacterial processes (45, 46) as an alternate Fe source that increases productivity and nitrogen uptake in food webs (47–49). Protozoa also engulf manganese-encrusted bacteria, which contributes to the geochemical cycling of Mn during normal protozoan bacterial digestion (50). Bioaccumulated thallium adsorbed to bacteria that are preyed upon by protozoa contributes to geochemical cycling through the oxidation of thermodynamically stable Tl(I) to more abundant Tl(III) (51). Here, the rather insoluble (20) TiO_2 nanomaterial was ingested and egested, as was the protozoan's food, and thus a greater proportion of the overall TiO_2 in the cultures was within the protozoans as their population size increased. Still, although biomagnification did not occur in our study, TiO_2 uptake was not beneficial to *T. thermophila* and in fact was slightly harmful on the population scale.

The ever-increasing use of manufactured TiO_2 increases the potential for population level impacts on organisms at the lowest trophic levels, which are fundamental to the overall health of ecosystems. Here, TiO_2 adsorbed to *P. aeruginosa* prey, which is a likely common association of manufactured nanomaterials with bacteria, was ingested along with *P. aeruginosa* during *T. thermophila* predation. In both regimens of TiO_2 intake (trophic transfer

and directly via medium) by *T. thermophila*, the main effects were the presence of TiO_2 in the *T. thermophila* population and a reduced population growth rate and yield. An implication is that, by their uptake into and growth effects on microbial food chains, nanomaterials could impact higher trophic levels irrespective of biomagnification.

ACKNOWLEDGMENTS

This research was funded primarily by the National Science Foundation and the Environmental Protection Agency under cooperative agreement DBI-0830117. Any opinions, findings, and conclusions or recommendations expressed in this material are ours and do not necessarily reflect the views of either the National Science Foundation or the Environmental Protection Agency. This work has not been subjected to Environmental Protection Agency review, and no official endorsement should be inferred.

ESEM and STEM were partly performed in the Micro-Environmental Imaging and Analysis Facility at the University of California Santa Barbara (www.bren.ucsb.edu/facilities/MEIAF/) under National Science Foundation awards BES-9977772 and DBI-0216480. Funding to E.O. was provided by National Science Foundation award MCB-1025069.

REFERENCES

1. **Klaine SJ, Alvarez PJJ, Batley GE, Fernandes TF, Handy RD, Lyon DY, Mahendra S, McLaughlin MJ, Lead JR.** 2008. Nanomaterials in the environment: behavior, fate, bioavailability, and effects. Environ. Toxicol. Chem. **27:**1825–1851.
2. **Lawton J.** 2008. Novel materials in the environment: the case of nanotechnology. Royal Commission on Environmental Pollution, London, United Kingdom.
3. **Kaegi R, Ulrich A, Sinnet B, Vonbank R, Wichser A, Zuleeg S, Simmler H, Brunner S, Vonmont H, Burkhardt M, Boller M.** 2008. Synthetic TiO_2 nanoparticle emission from exterior facades into the aquatic environment. Environ. Pollut. **156:**233–239.
4. **Weir A, Westerhoff P, Fabricius L, Hristovski K, von Goetz N.** 2012. Titanium dioxide nanoparticles in food and personal care products. Environ. Sci. Technol. **46:**2242–2250.
5. **Nohynek GJ, Antignac E, Re T, Toutain H.** 2010. Safety assessment of personal care products/cosmetics and their ingredients. Toxicol. Appl. Pharmacol. **243:**239–259.
6. **Choksi AN, Poonawalla T, Wilkerson MG.** 2010. Nanoparticles: a closer look at their dermal effects. J. Drugs Dermatol. **9:**475–481.
7. **Phillips LG, Barbano DM.** 1997. The influence of fat substitutes based on protein and titanium dioxide on the sensory properties of lowfat milks. J. Dairy Sci. **80:**2726–2731.
8. **Robichaud CO, Uyar AE, Darby MR, Zucker LG, Wiesner MR.** 2009. Estimates of upper bounds and trends in nano-TiO_2 production as a basis for exposure assessment. Environ. Sci. Technol. **43:**4227–4233.
9. **Boxall AB, Tiede K, Chaudhry Q.** 2007. Engineered nanomaterials in soils and water: how do they behave and could they pose a risk to human health? Nanomedicine **2:**919–927.
10. **Suresh AK, Pelletier DA, Doktycz MJ.** 2013. Relating nanomaterial properties and microbial toxicity. Nanoscale **5:**463–474.
11. **Mileyeva-Biebesheimer ON, Zaky A, Gruden CL.** 2010. Assessing the impact of titanium dioxide and zinc oxide nanoparticles on bacteria using a fluorescent-based cell membrane integrity assay. Environ. Eng. Sci. **27:** 329–335.
12. **Dumas EM, Ozenne V, Mielke RE, Nadeau JL.** 2009. Toxicity of CdTe quantum dots in bacterial strains. IEEE Trans. Nanobioscience **8:**58–64.
13. **Priester JH, Stoimenov PK, Mielke RE, Webb SM, Ehrhardt C, Zhang JP, Stucky GD, Holden PA.** 2009. Effects of soluble cadmium salts versus CdSe quantum dots on the growth of planktonic *Pseudomonas aeruginosa*. Environ. Sci. Technol. **43:**2589–2594.
14. **Kloepfer JA, Mielke RE, Wong MS, Nealson KH, Stucky G, Nadeau JL.** 2003. Quantum dots as strain- and metabolism-specific microbiological labels. Appl. Environ. Microbiol. **69:**4205–4213.
15. **Werlin R, Priester JH, Mielke RE, Krämer S, Jackson S, Stoimenov PK, Stucky GD, Cherr GN, Orias E, Holden PA.** 2011. Biomagnification of cadmium selenide quantum dots in a simple experimental microbial food chain. Nat. Nanotechnol. **6:**65–71.
16. **Ghafari P, St-Denis CH, Power ME, Jin X, Tsou V, Mandal HS, Bols NC, Tang X.** 2008. Impact of carbon nanotubes on the ingestion and digestion of bacteria by ciliated protozoa. Nat. Nanotechnol. **3:**347–351.
17. **Horst AM, Neal AC, Mielke RE, Sislian PR, Suh WH, Mädler L, Stucky GD, Holden PA.** 2010. Dispersion of TiO_2 nanoparticle agglomerates by *Pseudomonas aeruginosa*. Appl. Environ. Microbiol. **76:**7292–7298.
18. **Demchick P, Koch AL.** 1996. The permeability of the wall fabric of *Escherichia coli* and *Bacillus subtilis*. J. Bacteriol. **178:**768–773.
19. **Ohno T, Sarukawa K, Tokieda K, Matsumura M.** 2001. Morphology of a TiO_2 photocatalyst (Degussa, P-25) consisting of anatase and rutile crystalline phases. J. Catal. **203:**82–86.
20. **Keller AA, Wang HT, Zhou DX, Lenihan HS, Cherr G, Cardinale BJ, Miller R, Ji ZX.** 2010. Stability and aggregation of metal oxide nanoparticles in natural aqueous matrices. Environ. Sci. Technol. **44:**1962–1967.
21. **Kirk S, Skepper J, Donald AM.** 2009. Application of environmental scanning electron microscopy to determine biological surface structure. J. Microsc. **233:**205–224.
22. **Douglas S, Abbey W, Mielke R, Conrad P, Kanik I.** 2008. Textural and mineralogical biosignatures in an unusual microbialite from Death Valley, California. Icarus **193:**620–636.
23. **Priester JH, Ge Y, Mielke RE, Horst AM, Moritz SC, Espinosa K, Gelb J, Walker SL, Nisbet RM, An Y-J, Schimel JP, Palmer RG, Hernandez-Viezcas JA, Zhao L, Gardea-Torresdey JL, Holden PA.** 2012. Soybean susceptibility to manufactured nanomaterials with evidence for food quality and soil fertility interruption. Proc. Natl. Acad. Sci. U. S. A. **109:**E2451–E2456.
24. **Tkachuk A, Duewer F, Cui H, Feser M, Wang S, Yun W.** 2007. X-ray computed tomography in Zernike phase contrast mode at 8 keV with 50-nm resolution using Cu rotating anode X-ray source. Z. Kristallogr. **222:**650–655.
25. **Luoma SN, Rainbow PS.** 2008. Metal contamination in aquatic environments: science and lateral management. Cambridge University Press, Cambridge, United Kingdom.
26. **Arnot JA, Gobas F.** 2006. A review of bioconcentration factor (BCF) and bioaccumulation factor (BAF) assessments for organic chemicals in aquatic organisms. Environ. Rev. **14:**257–297.
27. **Luo ZX, Wang ZH, Li QZ, Pan QK, Yan CZ, Liu F.** 2011. Spatial distribution, electron microscopy analysis of titanium and its correlation to heavy metals: occurrence and sources of titanium nanomaterials in surface sediments from Xiamen Bay, China. J. Environ. Monit. **13:**1046–1052.
28. **Güde H.** 1979. Grazing by protozoa as selection factor for activated-sludge bacteria. Microb. Ecol. **5:**225–237.
29. **Sherr EB, Sherr BF.** 2002. Significance of predation by protists in aquatic microbial food webs. Antonie Van Leeuwenhoek **81:**293–308.
30. **Pernthaler J.** 2005. Predation on prokaryotes in the water column and its ecological implications. Nature Rev. Microbiology **3:**537–546.
31. **McGinness S, Johnson DB.** 1992. Grazing of acidophilic bacteria by a flagellated protozoan. Microb. Ecol. **23:**75–86.
32. **Johnson DB.** 1995. Acidophilic microbial communities: candidates for bioremediation of acidic mine effluents. Int. Biodeterior. Biodegradation **35:**41–58.
33. **Menon P, Becquevort S, Billen G, Servais P.** 1996. Kinetics of flagellate grazing in the presence of two types of bacterial prey. Microb. Ecol. **31:** 89–101.
34. **Boenigk J, Matz C, Jurgens K, Arndt H.** 2001. Confusing selective feeding with differential digestion in bacterivorous nanoflagellates. J. Eukaryot. Microbiol. **48:**425–432.
35. **Holbrook RD, Murphy KE, Morrow JB, Cole KD.** 2008. Trophic transfer of nanoparticles in a simplified invertebrate food web. Nat. Nanotechnol. **3:**352–355.
36. **Hou WC, Westerhoff P, Posner JD.** 2013. Biological accumulation of engineered nanomaterials: a review of current knowledge. Environ. Sci. Processes Impacts **15:**103–122.
37. **Deplanche K, Macaskie LE.** 2008. Biorecovery of gold by *Escherichia coli* and *Desulfovibrio desulfuricans*. Biotechnol. Bioeng. **99:**1055–1064.
38. **Sondi I, Salopek-Sondi B.** 2004. Silver nanoparticles as antimicrobial agent: a case study on *E. coli* as a model for Gram-negative bacteria. J. Colloid Interface Sci. **275:**177–182.
39. **Limbach LK, Bereiter R, Mueller E, Krebs R, Gaelli R, Stark WJ.** 2008. Removal of oxide nanoparticles in a model wastewater treatment plant: influence of agglomeration and surfactants on clearing efficiency. Environ. Sci. Technol. **42:**5828–5833.

40. **Lead JR, Davison W, Hamilton-Taylor J, Buffle J.** 1997. Characterizing colloidal material in natural waters. Aquat. Geochem. **3:**213–232.
41. **Guo L, Santschi PH.** 2007. Ultrafiltration and its applications to sampling and characterisation of aquatic colloids, p 159–221. *In* Wilkinson KJ, Lead JR (ed), Environmental colloids and particles: behaviour, separation and characterisation. John Wiley & Sons Ltd., West Sussex, United Kingdom.
42. **Zhu XS, Wang JX, Zhang XZ, Chang Y, Chen YS.** 2010. Trophic transfer of TiO_2 nanoparticles from daphnia to zebrafish in a simplified freshwater food chain. Chemosphere **79:**928–933.
43. **Gillan DC, Ribesse J, de Ridder C.** 2004. The iron-encrusted microbial community of *Urothoe poseidonis* (Crustacea, Amphipoda). J. Sea Res. **52:**21–32.
44. **Gillan DC, de Ridder C.** 1997. Morphology of a ferric iron-encrusted biofilm forming on the shell of a burrowing bivalve (Mollusca). Aquat. Microb. Ecol. **12:**1–10.
45. **Chase Z, Price NM.** 1997. Metabolic consequences of iron deficiency in heterotrophic marine protozoa. Limnol. Oceanogr. **42:**1673–1684.
46. **Wilson ME, Britigan BE.** 1998. Iron acquisition by parasitic protozoa. Parasitol. Today **14:**348–353.
47. **Kudo I, Noiri Y, Cochlan WP, Suzuki K, Aramaki T, Ono T, Nojiri Y.** 2009. Primary productivity, bacterial productivity and nitrogen uptake in response to iron enrichment during the SEEDS II. Deep-Sea Res. II **56:** 2755–2766.
48. **Christaki U, Obernosterer I, Van Wambeke F, Veldhuis M, Garcia N, Catala P.** 2008. Microbial food web structure in a naturally iron-fertilized area in the Southern Ocean (Kerguelen Plateau). Deep-Sea Res. II **55:**706–719.
49. **Vogel C, Fisher NS.** 2009. Trophic transfer of Fe, Zn and Am from marine bacteria to a planktonic ciliate. Mar. Ecol. Prog. Ser. **384:**61–68.
50. **Zeiner CA, Lion LW, Shuler ML, Ghirose WC, Hay A.** 2006. Cycling of biogenic Mn-oxides in a model microbial predator-prey system. Geomicrobiol. J. **23:**37–43.
51. **Twining BS, Twiss MR, Fisher NS.** 2003. Oxidation of thallium by freshwater plankton communities. Environ. Sci. Technol. **37:**2720–2726.